4-2018

Evaluation of a Hybrid Reflectance-Based Crop Coefficient and Energy Balance Evapotranspiration Model for Irrigation Management

J. Burdette Barker
University of Nebraska-Lincoln, burdette.barker@huskers.unl.edu

Christopher M. U. Neale
University of Nebraska-Lincoln, cneale@nebraska.edu

Derek M. Heeren
University of Nebraska-Lincoln, derek.heeren@unl.edu

Andrew E. Suyker
University of Nebraska - Lincoln, asuyker1@unl.edu

EVALUATION OF A HYBRID REFLECTANCE-BASED CROP COEFFICIENT AND ENERGY BALANCE EVAPOTRANSPIRATION MODEL FOR IRRIGATION MANAGEMENT

J. B. Barker, C. M. U. Neale, D. M. Heeren, A. E. Suyker

ABSTRACT. *Accurate generation of spatial soil water maps is useful for many types of irrigation management. A hybrid remote sensing evapotranspiration (ET) model combining reflectance-based basal crop coefficients (K_{cbrf}) and a two-source energy balance (TSEB) model was modified and validated for use in real-time irrigation management. We modeled spatial ET for maize and soybean fields in eastern Nebraska for the 2011-2013 growing seasons. We used Landsat 5, 7, and 8 imagery as remote sensing inputs. In the TSEB, we used the Priestly-Taylor (PT) approximation for canopy latent heat flux, as in the original model formulations. We also used the Penman-Monteith (PM) approximation for comparison. We compared energy balance fluxes and computed ET with measurements from three eddy covariance systems within the study area. Net radiation was underestimated by the model when data from a local weather station were used as input, with mean bias error (MBE) of -33.8 to -40.9 W m^{-2}. The measured incident solar radiation appeared to be biased low. The net radiation model performed more satisfactorily when data from the eddy covariance flux towers were input into the model, with MBE of 5.3 to 11.2 W m^{-2}. We removed bias in the daily energy balance ET using a dimensionless multiplier that ranged from 0.89 to 0.99. The bias-corrected TSEB ET, using weather data from a local weather station and with local ground data in thermal infrared imagery corrections, had MBE = 0.09 mm d^{-1} (RMSE = 1.49 mm d^{-1}) for PM and MBE = 0.04 mm d^{-1} (RMSE = 1.18 mm d^{-1}) for PT. The hybrid model used statistical interpolation to combine the two ET estimates. We computed weighting factors for statistical interpolation to be 0.37 to 0.50 for the PM method and 0.56 to 0.64 for the PT method. Provisions were added to the model, including a real-time crop coefficient methodology, which allowed seasonal crop coefficients to be computed with relatively few remote sensing images. This methodology performed well when compared to basal crop coefficients computed using a full season of input imagery. Water balance ET compared favorably with the eddy covariance data after incorporating the TSEB ET. For a validation dataset, the magnitude of MBE decreased from -0.86 mm d^{-1} (RMSE = 1.37 mm d^{-1}) for the K_{cbrf} alone to -0.45 mm d^{-1} (RMSE = 0.98 mm d^{-1}) and -0.39 mm d^{-1} (RMSE = 0.95 mm d^{-1}) with incorporation of the TSEB ET using the PM and PT methods, respectively. However, the magnitudes of MBE and RMSE were increased for a running average of daily computations in the full May-October periods. The hybrid model did not necessarily result in improved model performance. However, the water balance model is adaptable for real-time irrigation scheduling and may be combined with forecasted reference ET, although the low temporal frequency of satellite imagery is expected to be a challenge in real-time irrigation management.*

Keywords. *Center-pivot irrigation, ET estimation methods, Evapotranspiration, Irrigation scheduling, Irrigation water balance, Model validation, Variable-rate irrigation.*

Multispectral remote sensing-based evapotranspiration (ET) models have been studied for use in irrigation management for decades (Neale et al., 1989; Hunsaker et al., 2005; Campos et al., 2010). Remote sensing-based ET models have the benefit of representing local crop conditions (Bausch and Neale, 1987). Remote sensing imagery has been successfully implemented to estimate ET at varying spatial scales (e.g., Allen et al., 2007a; Neale et al., 2012). Remote-sensing ET models may be particularly well suited for application in variable-rate irrigation (VRI), where irrigation is managed for individual subareas (or zones) within a field. Some recent research has focused on remote or proximal sensing of crop status for VRI management (e.g., O'Shaughnessy et al., 2015; Stone et al., 2016).

Two types of remote sensing ET estimation techniques are (surface) energy balance models and reflectance-based crop coefficient (K_{cbrf}) models. Energy balance techniques use shortwave reflectance and thermal infrared imagery to estimate available energy (R_n–G) and sensible heat flux (H). Latent heat flux (LE) may be taken as the residual balance

Submitted for review in February 2017 as manuscript number NRES 12311; approved for publication by the Natural Resources & Environmental Systems Community of ASABE in September 2017.

The authors are **J. Burdette Barker,** Post-Doctoral Research Associate, Department of Biological Systems Engineering, **Christopher M. U. Neale,** Professor and Director of Research, Daugherty Water for Food Global Institute at the University of Nebraska, **Derek M. Heeren,** Assistant Professor and Daugherty Water for Food Global Institute Faculty Fellow, Department of Biological Systems Engineering, and **Andrew E. Suyker,** Associate Professor and Daugherty Water for Food Global Institute Faculty Fellow, School of Natural Resources, University of Nebraska-Lincoln, Lincoln, Nebraska. **Corresponding author:** J. Burdette Barker, 102 L. W. Chase Hall, 3605 Fair St., University of Nebraska, Lincoln, NE 68583-0726; phone: 402-472-1413; e-mail: burdette.barker@huskers.unl.edu.

  ISSN 2151-0032 https://doi.org/10.13031/trans.12311

between the two (Neale et al., 2012). Neale et al. (2012) and Gowda et al. (2007) discussed the differences between different remote-sensing-based ET models in further detail. In the two-source energy balance method (TSEB) originally developed by Norman et al. (1995), the soil and plant contributions to energy fluxes are considered separately rather than as a combined surface (hence two sources). Neale et al. (2012) commented on the advantage of TSEB over other methods. However, when applied using satellite imagery, the TSEB method does require atmospherically corrected thermal infrared imagery (Neale et al., 2012). As not all thermal infrared products include atmospheric corrections, this may require additional processing by the user. Furthermore, the requirement of input thermal infrared imagery into the model may limit the use of the model to times when imagery is available.

In the K_{cbrf} approach, crop ET (ET_c) is computed using reference ET (ET_r) and a dual crop coefficient, which is as follows based on FAO Irrigation and Drainage Paper No. 56 (FAO-56; Allen et al., 1998):

$$ET_c = (K_{cb}K_s + K_e)ET_r \quad (1)$$

where K_{cb} is a basal crop coefficient, K_s is a water stress coefficient, and K_e is a soil evaporation coefficient. The K_{cbrf} approach uses vegetation indices, such as the normalized difference vegetation index (NDVI; Rouse et al., 1974) or the soil-adjusted vegetation index (SAVI; Huete, 1988), from shortwave reflectance imagery to determine K_{cb} (Bausch and Neale, 1987; Neale et al., 1989; Bausch, 1993).

Campos et al. (2010) found that a model using K_{cbrf}-ET compared well with eddy covariance ET measurements for irrigated grapes. Hunsaker et al. (2005) used a K_{cbrf} method and a traditional, time-based K_{cb} approach to schedule irrigations for cotton of varying stand densities and nitrogen treatments. They found that the traditional method outperformed the K_{cbrf} method (in terms of irrigation adequacy and yield) in the first year of their study. In the subsequent year, both methods were site-adjusted and both performed similarly, on average, although the K_{cbrf} method performed better when stand density was taken into consideration. Their results demonstrate the utility of the K_{cbrf} method and a potential need for local calibration. Stone et al. (2016) used NDVI-based K_{cbrf} values and FAO-56 methodologies (Allen et al., 1998) to manage VRI in maize in South Carolina. This method performed similarly to irrigation management based on measurements of soil water potential.

The Spatial EvapoTranspiration Modelling Interface (SETMI) developed by Geli and Neale (2012) includes a hybrid of the TSEB method and a K_{cbrf}-based water balance method (Neale et al., 2012). The K_{cbrf} portion of the model allows ET to be computed within and extrapolated beyond the input image date range because a full-season K_{cb} may be computed from relatively infrequent or few images (Neale et al., 2012). Thus, a daily water balance may be computed for use in real-time irrigation scheduling. The inclusion of the TSEB method provides a self-adjusting capability to the model (Neale et al., 2012). The K_{cbrf}-ET is dependent on the accuracy of the water balance model in predicting K_s and K_e components of the estimated ET (Allen et al., 1998). For instance, errors in water balance inputs and assumptions could provide undesired feedback into the model. This is of particular concern if irrigation is scheduled based on the modeled soil water depletion. The TSEB provides a spatial estimate of ET at the time an image is taken that is independent of the water balance (Neale et al., 2012), except in sharing shortwave reflectance imagery and weather data. In this way, the water balance can be adjusted when each new image is incorporated into the model.

We hypothesize that the hybrid model represents an improvement over using either the TSEB or K_{cbrf} alone (see Neale et al., 2012) and is thus well suited for irrigation management. Irrigation prescriptions development with the SETMI interface have the potential to account for spatially variable water requirements with the added benefit of incorporating multispectral imagery as an indirect indication of actual crop status. The modeled spatial water balance could then be applied to VRI or traditional irrigation methods.

OBJECTIVES

The objective of this research was to determine whether the hybrid model in SETMI was well suited for ET modeling in eastern Nebraska, with the ultimate intent being application in real-time irrigation management. This was accomplished by validating and calibrating the TSEB energy flux and ET and water balance ET estimates from SETMI for three years for an experimental area near Mead, Nebraska, with eddy covariance energy flux data. Some additions to the SETMI program are also discussed herein.

METHODS

MODEL FORMULATIONS

The hybrid model (Neale et al., 2012) was implemented within the SETMI interface (Geli and Neale, 2012). The SETMI interface as employed here operated as a tool within ArcGIS 10.4. The version of SETMI used herein was modified by us. Modifications were made to both the water balance and TSEB models.

Two-Source Model

The original formulation of the TSEB used the Priestly-Taylor (PT) equation to approximate canopy latent heat flux (LE_c; Norman et al., 1995). This is given in equation 2, following notation similar to Colaizzi et al. (2014), and solved for canopy sensible heat flux (H_c) as in Norman et al. (1995). The sign convention of $R_{nc} = H_c + LE_c$, where R_{nc} is the canopy portion of net radiation is followed:

$$H_c = R_{nc}\left[1 - \alpha_{PT} f_g \left(\frac{\Delta}{\Delta + \gamma}\right)\right] \quad (2)$$

where α_{PT} is a constant, f_g is the fraction of green leaf area, Δ is the slope of the vapor pressure-temperature curve, and γ is the psychrometric constant. In this study, α_{PT} was given an initial value of 1.26 (Kustas and Norman 1997), which was reduced in 0.01 increments until the energy balance was satisfied, as programmed by Geli et al. (2014); see also Li et al. (2005).

We modified the TSEB in SETMI to optionally include the Penman-Monteith (PM) approximation of LE_c following Colaizzi et al. (2014). This is equation 3 when solved for H_c and following the previously mentioned sign convention:

$$H_c = R_{nc} - f_g\left[\left(\frac{\Delta}{\Delta+\gamma^*}\right)R_{nc} + c_{pm}\rho_m\frac{(e_s-e_a)}{r_a(\Delta+\gamma^*)}\right] \quad (3)$$

where c_{pm} is the specific heat of moist air, ρ_m is the density of moist air, e_s and e_a are the saturated and actual vapor pressures, respectively, r_a is the aerodynamic resistance to heat transfer, and γ^* is given, following Colaizzi et al. (2012b), as $\gamma^* = \gamma(1 + r_c/r_a)$, where r_c is the bulk canopy resistance. The r_c was set to an initial value of 50 s m^{-1} and adjusted to prevent negative soil latent heat flux as in Colaizzi et al. (2012b). In computing Δ and γ, we used the average of air temperature and canopy temperature, applying an iterative solution similar to Colaizzi et al. (2016), except that we included the process for γ in addition to Δ.

Other notable additions to the TSEB model in SETMI included provisions to enable better model performance during senescence. The model computed leaf area index (LAI) and crop height using the optimized soil-adjusted vegetation index (Rondeaux et al., 1996) and relationships reported by Anderson et al. (2004). It computed f_c using the equation of Choudhury et al. (1994) similar to Li et al. (2005):

$$f_c = 1 - \left(\frac{VI_x - VI}{VI_x - VI_n}\right)^c \quad (4)$$

where VI is a vegetation index, in this case the normalized difference vegetation index (NDVI), the subscripts x and n represent maximum and minimum, respectively, and c is a constant. NDVI$_x$ and NDVI$_n$ were set to 0.9 and 0.2, respectively, and c was hard coded in SETMI as 0.7 (Geli et al., 2014).

When vegetation indices decrease with senescence, the modeled vegetation-index-based LAI, crop height, and f_c also decrease. We added the capability to input LAI, crop height, and f_c for previous dates to the model. The model was then able to maintain the peak LAI, height, and/or f_c during senescence. We also computed f_g as the fraction of current date LAI to peak LAI. This was similar to the work of Houborg et al. (2009), who computed f_g as the fraction of current LAI over average LAI during the peak period. In model implementation, we computed f_g this way for all images in September and October. We maintained crop height at the peak crop height for all images after peak (practically applied after early July). We did not incorporate the peak nadir f_c option because it did not improve model results in preliminary analysis.

Vegetation absorptivities used in the net radiation (R_n) model (Campbell and Norman, 2012) for the TSEB are listed in table 1. Soil heat flux (G) was computed as 0.3(R_{ns}) following Norman et al. (1995), but using 0.3 as recommended by Brutsaert (1982) for use with bare soil. For vegetation clumping (Kustas and Norman, 1999), we assumed canopy widths of 0.76 m in all cases, even low cover. Temporal scaling of LE to daily ET followed one method of Chavez et al. (2008):

$$\mathrm{ET}_d = LE_i\left(\frac{3600}{\lambda}\right)\left(\frac{\mathrm{ET}_{r,d}}{\mathrm{ET}_{r,i}}\right) \quad (5)$$

where the subscripts d and i are for daily and instantaneous values, respectively. The units for the constant are s mm m^2 h^{-1} kg^{-1} with LE_i in W m^{-2}, λ in J kg^{-1}, ET$_{r,i}$ in mm h^{-1}, and daily ET$_d$ and ET$_{r,d}$ in mm d^{-1}. We computed λ following Ham (2005).

Table 1. Net radiation parameters used in the two-source model for both maize and soybeans.

Surface	Absorptivity		Emissivity
	Visible	Near-Infrared	
Green vegetation	0.85[a]	0.20[b]	0.98[b]
Senesced vegetation	0.49[c]	0.13[c]	0.95[d]
Soil	0.15[a]	0.25[a]	0.96[c]

[a] Source: Colaizzi et al. (2012a).
[b] Source: Brunsell and Gillies (2002).
[c] Source: Houborg et al. (2009).
[d] Default for corn and soybeans in SETMI (Geli et al., 2014).

Water Balance Model

In the water balance model, crop coefficients were obtained from reflectance data using the SAVI-to-K_{cbrf} relationships developed by Campos et al. (2017): $K_{cbrf} = a(\mathrm{SAVI}) + b$, where a and b were 1.414 and -0.020, respectively, for maize and 1.258 and -0.006, respectively, for soybean. The regression method of Campos et al. (2017) was used to produce daily K_{cb} values. This method can be given as:

$$\mathrm{SAVI}_j = \min\left[\exp(a_1\mathrm{CGDD}_j + b_1),\ \mathrm{SAVI}_x\exp\left(-\exp(a_2\mathrm{CGDD}_j + b_2)\right)\right] \quad (6)$$

where SAVI$_j$ is the estimated SAVI for the current day, SAVI$_x$ is a maximum SAVI, taken here to be the peak computed value for a given pixel, CGDD$_j$ is the cumulative growing degree days for the current day (NDAWN, 2017), a and b are linear regression coefficients, and the subscripts 1 and 2 represent the two stages of growth described in figure 1.

The focus of the current analysis was to improve and test the model for real-time irrigation scheduling. As future images are not available in real-time application, functionality was added to enable computation of the K_{cb} beyond the most

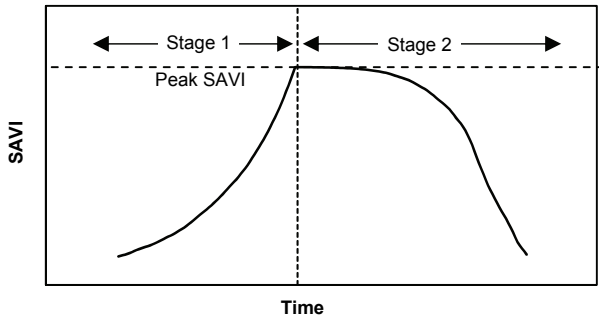

Figure 1. Idealized SAVI curve showing stages used in computing SAVI regression coefficients with form based on Campos et al. (2017) and stages defined by us.

recent input image date. This methodology included two parts: (1) a forecasted peak SAVI value and (2) a projected end of season SAVI. Both values were model inputs; the former also required input of an upper bound day-of-year for which the peak could occur; and the latter the day-of-year on which to apply the value.

In forecasting the peak SAVI, a minimum of two reflectance images during stage 1 (fig. 1) crop development were required to compute the daily SAVI estimates. The SAVI values were then computed for the stage 1 portion of the season using equation 6. The forecasted day-of-peak-SAVI was computed as the day on which SAVI exceeded the input forecasted SAVI value or the input upper bound day-of-year, whichever was earlier. A forecasted SAVI slightly smaller than the peak (e.g., 0.999 times the input forecast peak value) was then inserted on this forecasted peak day and became the first day of the stage 2 curve. The input forecasted peak SAVI value was used as $SAVI_x$ as defined in equation 6. The aforementioned slight reduction in SAVI following the projected peak prevented a calculation error (eq. 6). In the event that a forecasted peak SAVI was input and an image with a SAVI value greater than the forecasted peak occurred, the projected peak date was still used, but $SAVI_x$ was taken to be slightly larger than the actual peak SAVI. Again, this was to prevent a logarithm error (eq. 6).

The projected end-of-season SAVI represented mature, senesced, or harvested conditions (depending on the crop and modeling conditions). This allowed the stage 2 portion of the SAVI curve to decrease at an appropriate rate, with the end of the season having a more realistic performance than if only imagery early in stage 2 were included. The projected end-of-season SAVI was imposed on the corresponding input projected end-SAVI day-of-year. In a given season, as more reflectance images became available, the intent was that the forecasted peak and end SAVI values would only be used until sufficient imagery were obtained so that the projected values were no longer needed to produce the K_{cb}.

In computing the daily SAVI values, a final constraint was applied so that no images after day-of-year 232 (a changeable input value) were allowed to be considered in stage 1 of the curve (fig. 1). This is because in years with sparse imagery, such as 2012 and 2013, it is possible to have a peak SAVI from the imagery that occurs well after effective full cover. This can cause the stage 1 portion of the SAVI to be stretched out unreasonably late in the season. When this constraint was imposed, $SAVI_x$ was computed to be slightly larger than the actual peak SAVI from the imagery to prevent a calculation error. In the ET comparisons herein, only this final constraint was applied, the forecasting methods were not.

The water balance model itself generally followed FAO-56 (Allen et al., 1998), not including some of the methods described by Jensen and Allen (2016). Some notable exceptions to the methodology are detailed here. Tall reference ET_r was used; soil evaporation was therefore modeled similarly to Allen et al. (2007b). We used a maximum root zone depth of 1.2 m for maize and 1.0 m for soybean. We assumed an evaporative layer depth of 0.05 m. The evaporation model requires an estimate of f_c (Allen et al., 1998). The SETMI water balance model was modified to compute f_c using the equation of Choudhury et al. (1994) as in equation 4, but using SAVI for the *VI* instead of NDVI and using an exponent (c) value of 1 per the discussion of Choudhury et al. (1994) and limits as in Allen et al. (1998). The maximum and minimum values of SAVI were set to 0.68 and 0.12, respectively, based on the K_{cb} relationships of Campos et al. (2017), particularly that for maize, and in the case of the 0.68 value, based on a spreadsheet provided by I. Campos (personal communication, April 4, 2016); see also Campos et al. (2017).

Some other model parameterizations are provided here. A minimum root zone depth of 0.1 m was assumed for both crops. The fraction of depletion before water stress occurred was assumed to be 0.55 and 0.5 for maize and soybeans, respectively. These values were adjusted for evaporative demand as in Allen et al. (1998). The water balance was run from day 120 to 305, approximately April through October. Other model parameterizations included effective rainfall and irrigation computations. We used the USDA Natural Resources Conservation Service runoff equation (USDA, 2004) to compute rainfall runoff with a curve number of 80. We assumed an application efficiency of 90% in computing net irrigation.

Hybrid Model

In the hybrid methodology, the TSEB ET was incorporated using the simplified statistical interpolation equation presented in the form of (Neale et al., 2012):

$$ET^{A}_{WB} = ET^{B}_{WB} + W\left(ET_{TSEB} - ET^{B}_{WB}\right) \quad (7)$$

where ET^{A}_{WB} is the water balance ET after including the TSEB ET (ET_{TSEB}), ET^{B}_{WB} is the water balance ET before the incorporation, and W is a Kalman gain. This gain was computed using the error variance of the water balance and TSEB ET following Neale et al. (2012) and H. Geli (personal communication). Differences between ET^{A}_{WB} and ET^{B}_{WB} were attributed to modeled water stress (K_s in eq. 1; Geli, 2012). This was done by back-calculating for K_s using equation 1 and substituting ET^{A}_{WB} for ET_c (Geli, 2012). The modeled previous day root zone depletion (Allen et al., 1998) after incorporating TSEB ET (D^{A}_{rLast}) was then computed following Geli (2012) and Geli et al. (2014) by rearranging equation 84 of Allen et al. (1998) as D^{A}_{rLast} = TAW – K_s(TAW – RAW), where TAW and RAW are total and readily available water, respectively. Finally, D^{A}_{rLast} was limited to be ≥ 0 (Geli et al., 2014).

For actual TSEB ET incorporation, a constraint was added for cases where neither model indicated water stress. The constraint was as follows: if TSEB ET was greater than water balance ET, and the water balance did not indicate water stress (K_s = 1), then no adjustment was made to the root zone depletion. However, ET^{A}_{WB} was still used for the water balance computations. Without this logic, the incorporation method would compute D^{A}_{rLast} to be at the brink of water stress in this condition. In reality, there was no justification for adjusting the soil water depletion in such a case. The ability to similarly incorporate soil water content measurements into the model was also added, although it was beyond the scope of the current research to test. With this addition, root zone depletion, evaporated depth, and lower layer soil water content may be incorporated using statistical interpolation, as for actual ET (eq. 7). Each dataset may have its own unique W (eq. 7).

Model Validation

Research Sites

The research for this study focused on three fields approximately 50 to 65 ha in size, planted in maize and maize-soybean crop rotations under irrigated and rainfed management, located at the University of Nebraska Eastern Nebraska Research and Extension Center (ENREC) near Mead, Nebraska (fig. 2). Soils are predominantly silt loam and silty clay loam series (Soil Survey Staff, 2016b). Three eddy covariance systems have been maintained as part of the University of Nebraska's Carbon Sequestration Project (CSP) at the site since 2001 (e.g., Suyker et al., 2004). Energy fluxes from the three sites were used to validate the hybrid model. A summary of the crops and cropping dates for the three CSP sites is presented in table 2.

Eddy Covariance Data

Energy flux measurements were obtained for the three eddy covariance (EC) systems within the study area, one in each field listed in table 2. The EC systems are hereafter referred to using the field names in table 1. These EC systems were part of the previously mentioned CSP project (Suyker et al., 2004; Suyker and Verma, 2009), and data are available through the AmeriFlux program (USDOE, 2017a), through which the 2011 and 2012 flux data were obtained. AmeriFlux site names for CSP1, CSP2, and CSP3 are US-Ne1 (Suyker, 2018a), US-Ne2 (Suyker, 2018b), and US-Ne3 (Suyker, 2018c), respectively (USDOE, 2017b). Each station was equipped with a 3D research anemometer (model R3, Gill Instruments, Lymington, U.K.), an open-path CO_2/H_2O analyzer (LI7500, Li-Cor Biosciences, Lincoln, Neb.), a net radiometer (CNR 1, Kipp & Zonen, Delft, The Netherlands), and soil heat flux plates (HFT3, Radiation and Energy Balance Systems, Inc., Seattle, Wash.) (Suyker et al., 2004). Aerodynamic sensors were mounted at 6.2 m above the ground surface when the crop was more than 1 m tall in maize and 3 m above the ground surface otherwise (Suyker et al., 2004). Net radiometers were mounted 5.5 m above the ground surface, and soil heat flux plates were installed at a depth of 6 cm (Suyker et al., 2004). Eddy covariance corrections were applied as in Suyker and Verma (2009). Missing data were filled as in Suyker and Verma (2009).

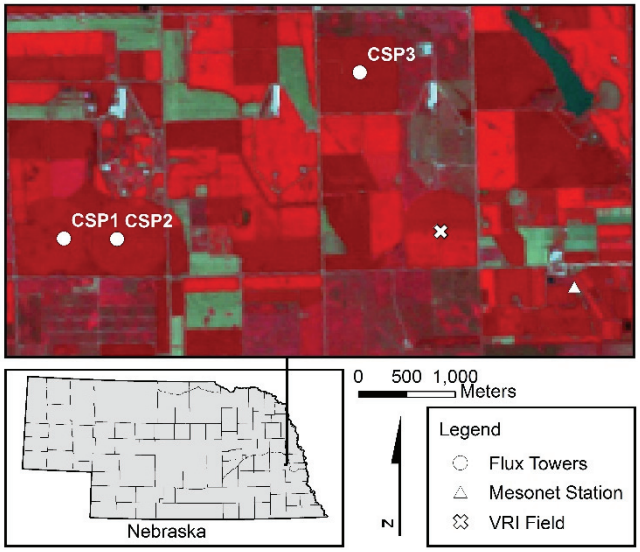

Figure 2. Study area map with August 1, 2011, Landsat 5 false color surface reflectance image background. Nebraska county map source: USDA (2009b). Nebraska state map source: USDA (2009a). The flux towers are CSP1 (irrigated continuous maize), CSP2 (irrigated maize-soybean rotation), and CSP3 (rainfed maize-soybean rotation). Locations of flux towers were obtained from USDOE (2017c, 2017d, 2017e). Location of the Nebraska Mesonet station is from G. Roebke and J. Buescher (personal communication, September 24, 2014).

Table 2. Summary of cropping system information for three fields with eddy covariance systems.

Field[a]	Year	Crop	Planting	Harvest
CSP1	2011	Maize	May 17	Oct. 26-27
	2012	Maize	Apr. 23	Oct. 10-11
	2013	Maize	Apr. 29	Oct. 22-23
CSP2	2011	Maize	May 17	Oct. 26-28
	2012	Maize	Apr. 24	Oct. 9-10
	2013	Maize	Apr. 30	Oct. 22-23
CSP3	2011	Maize	May 2	Oct. 18
	2012	Soybean	May 15	Oct. 1
	2013	Maize	May 13	Nov. 21-22

[a] CSP1 = irrigated continuous maize, CSP2 = irrigated maize-soybean rotation, and CSP3 = rainfed maize-soybean rotation.

Eddy covariance energy balance closure was forced for all analyses in this study. That is, H and LE were adjusted proportionally to satisfy $R_n - G = H + LE$, similar to Twine et al. (2000). In forcing closure, limits were imposed on the amount of adjustment that could be applied to H and LE. These limits were determined based on daytime ($R_n > 50$ W m^{-2}) fluxes between day-of-year 120 and 305 (roughly May through October) for 2011-2013. Twine et al. (2000) used the same R_n criterion for identifying daytime fluxes. Upper and lower limits of the mean ratio of energy balance closure of forced H and LE over non-forced fluxes were imposed in the closure forcing process. These limits were computed using the inner 95% probability values (assuming a normal distribution). The imposed upper and lower bounds were about 0.05 to 2.52 times the non-forced flux.

Campos et al. (2017) used data from these EC systems to develop their K_{cbrf} and daily SAVI estimation methodology, including data from 2011 and 2012, also used here. However, we did not follow the exact water balance formulations and parameterizations that Campos et al. (2017) used, and we forced EC energy balance closure, as mentioned above, while they used different methodology

Satellite Imagery

Imagery from Landsat 5 Thematic Mapper (TM), Landsat 7 Enhanced Thematic Mapper Plus (ETM+), and Landsat 8 Operational Land Imager (OLI) and Thermal Infrared Sensor (TIRS) were obtained from the U.S. Geological Survey ("data available from the U.S. Geological Survey"; https://lta.cr.usgs.gov/citation) for a combined total of 22 overpasses in the 2011 to 2013 growing seasons. Pre-collection Landsat imagery were used for this study (USGS EROS User Services, personal communication, September 21, 2017). Imagery dates are listed in table 3. Four of the images were excluded from TSEB computations because of insufficient green vegetative cover early or late in the growing season. We anticipated that the function of the model at higher vegetation cover was most pertinent, particularly in maize and soybean systems. Additional filtering was applied during analysis to exclude TSEB results if the comparison pixels

Table 3. Landsat images included in the study near Mead, Nebraska.

Date	Satellite	WB[a]	TSEB[b]
6 June 2011	Landsat 7	x	-
30 June 2011	Landsat 5	x	x
8 July 2011	Landsat 7	x	x
24 July 2011	Landsat 7	x	x
1 Aug. 2011	Landsat 5	x	x
9 Aug. 2011	Landsat 7	x	x
17 Aug. 2011	Landsat 5	x	x
25 Aug. 2011	Landsat 7	x	x
2 Sept. 2011	Landsat 5	x	x
10 Sept. 2011	Landsat 7	x	x
4 Oct. 2011	Landsat 5	x	x
8 June 2012	Landsat 7	x	x
24 June 2012	Landsat 7	x	x
10 July 2012	Landsat 7	x	x
26 July 2012	Landsat 7	x	x
27 Aug. 2012	Landsat 7	x	x
14 Oct. 2012	Landsat 7	x	-
3 June 2013	Landsat 8	x	-
11 June 2013	Landsat 7	x	x
21 July 2013	Landsat 8	x	x
23 Sept. 2013	Landsat 8	x	x
9 Oct. 2013	Landsat 8	x	-

[a] Imagery included in water balance computations.

[b] Imagery included in two-source energy balance computations. October 9, 2013, was included in TSEB computations but excluded from analysis because of low vegetative cover. Individual fields were excluded based on fraction of vegetative cover also, including: CSP1 11 June 2013, and CSP3 4 Oct. 2011, 8 June 2012, and 11 June 2013.

had a computed nadir fraction of vegetative cover (f_c) less than 0.2. This is within the range of minimum cover observed in other studies, e.g., 25% or greater in (Li et al., 2005) and 17% or greater in Colaizzi et al. (2012b). The f_c was computed using equation 4 and associated text.

Landsat surface reflectance products were provided through the courtesy of the U.S. Geological Survey ("data available from the U.S. Geological Survey"; https://lta.cr.usgs.gov/citation). Landsat thermal infrared imagery was corrected for atmospheric interference using parameters calculated with the Atmospheric Correction Parameter Calculator web application (Barsi et al., 2003; Barsi, 2018). Correction parameters were computed for atmospheric profiles that were spatially interpolated to the location of a local electronic weather station described later. For comparison, correction parameters were computed using profiles that both did and did not include input of local surface weather data from the weather station. Surface emissivities for the corrections were calculated following Brunsell and Gillies (2002). Surface emissivity was computed using linear scaling-based f_c between bare surface emissivity (0.96; Houborg et al., 2009) and vegetation emissivity (0.98; Brunsell and Gillies, 2002). The f_c equation used by Brunsell and Gillies (2002) was:

$$f_c = \left(\frac{VI - VI_n}{VI_x - VI_n} \right)^2 \quad (8)$$

Again, NDVI was used as the VI, with $NDVI_x$ and $NDVI_n$ as listed for equation 4. Atmospheric and emissivity (Neale et al., 2012) corrections were applied using ERDAS Imagine 2014 (Hexagon Geospatial, Madison, Ala.).

The ground spatial resolution of shortwave bands for Landsat 5, 7, and 8 is 30 m (USGS, 2016). The spatial resolution of the thermal infrared imagery is 120 m for Landsat 5, 60 m for Landsat 7, and 100 m for Landsat 8 (USGS, 2016). All thermal infrared imagery was resampled to 30 m for the commonly available data products (USGS, 2016). This resolution is likely too coarse for some precision agriculture activities. However, this resolution may be adequate for many irrigation applications, including some VRI applications. For example, Higgins et al. (2016) found that the minimum management zone size, for which the center of the zone might receive the intended application rate, was 23 m for a certain VRI-equipped center pivot.

Soil Properties and Land Cover

The SETMI interface requires the input of land use classifications and soil property data. The land use was classified manually using outlines of the study fields that were based on USDA aerial imagery (USDA, 2012).

The required soil data included field capacity (FC), permanent wilting point (WP), and initial profile-average volumetric water content maps as model inputs. Wilting point was obtained from the USDA-NRCS Soil Survey Geographic (SSURGO) database (Soil Survey Staff, 2016a). Soil survey shape files were converted into 30 m raster files for input into SETMI using ArcGIS 10.4 (ESRI, Redlands, Cal.). The SSURGO data were collected at a "mapping scale" of 1:12,000 to 1:63,360 (metadata associated with SSURGO database; Soil Survey Staff, 2016a), which is admittedly coarse for precision agriculture or VRI management. However, the dataset was used for this study because of the impracticality of obtaining higher-resolution soil property information for the entire study area. Field capacity was assumed to be 400 mm m^{-1} over the entire study area based on pre-planting neutron probe soil water content observations in a nearby VRI field (fig. 2) (Barker et al., 2018). Initial profile-average water content on day-of-year 120 was assumed to be at FC. We generally considered the soils at this site to be at FC in the spring (D. L. Martin, personal communication). Rainfall at the local weather station in April ranged from about 82 to 93 mm during the study, and May rainfall ranged from about 80 to 161 mm. Furthermore, the earliest irrigation events (not including fertigation, testing, etc.) were in early June (in 2012, the dry year) during the study.

Weather Data

The SETMI model requires ground-based point and/or raster weather data. The TSEB requires instantaneous values of air temperature, incident solar radiation, wind speed, vapor pressure, and barometric pressure. Instantaneous and daily total ET_r were also input to scale modeled instantaneous LE to daily ET values (eq. 5). The water balance requires input of daily total ET_r, precipitation, gross irrigation, and maximum and minimum daily air temperatures. Irrigation data were obtained from management records; although there was some uncertainty in the data, we feel the final values used herein were accurate enough for our purposes. We used point weather data obtained from the High Plains Regional Climate Center for the Nebraska Mesonet's Memphis 5N weather station, located within the study area (fig. 1). Barometric pressure data were obtained from a COsmic-ray Soil Moisture Observing System (COSMOS; Zreda et al.,

2012) site located in the CSP3 field (COSMOS, 2017). The ET_r was calculated with an hourly time step using the ASCE standardized reference ET equation for a tall reference crop (ASCE, 2005). Wind speed was adjusted to reference conditions (ASCE, 2005), similar to Allen and Wright (1997). We assumed a fetch length of 400 m, and vegetation to be about 0.5 m both regionally and in the vicinity of the weather station. A similar wind adjustment was performed in computing the TSEB; however, wind speed was adjusted to represent values measured over the modeled crops using modeled crop height and the assumed 400 m fetch length. We acknowledge that this adjustment methodology does not account for atmospheric stability (Allen and Wright, 1997; R. G. Allen, personal communication, June 22, 2017).

We observed that the solar radiation records from the Memphis 5N weather station were typically lower than the modeled clear-day solar radiation (ASCE, 2005) and solar radiation measured at the eddy covariance flux towers. However, the weather station pyranometers had been replaced approximately annually (S. Cooper, personal communication, January 13, 2017). There was also concern about the accuracy of adjusting the wind speed measured at the weather station to be representative of that over the crops. Thus, we also included weather data measured at the flux towers in the modeling. The TSEB and water balance were both computed with both datasets. In this study, weather data from a particular flux field were used only for that field; however, precipitation inputs for the flux tower dataset were taken only from CSP3 (the rainfed site, which had no irrigation data in the precipitation record). In computing reference ET using the flux tower data, we adjusted the wind speed data similarly to Allen and Wright (1997), using fetch lengths for measured and modeled surfaces of 400 m, an assumed regional vegetation height of 0.5 m, and crop height datasets provided by A. E. Suyker for each of the respective CSP fields.

No adjustments were applied to the flux tower wind speed data when used in the TSEB model fluxes. In using the flux tower datasets, some minor gap filling of air temperature and relative humidity was needed beyond that provided in the AmeriFlux datasets. This was done using the average of data from the nearest adjacent hour with data before and after the gap. Maximum and minimum daily air temperatures for the flux tower datasets were computed from hourly averages and were assumed adequate for growing degree day computations.

Model Performance

The TSEB model was validated using the PT approximation, per the original model development (Norman et al., 1995). The TSEB was also validated using the PM method (Colaizzi et al., 2014). The TSEB was computed using thermal infrared imagery that was corrected by both using and not using local ground weather data, as described earlier. The TSEB was also computed using both weather datasets.

The water balance was computed with and without TSEB ET incorporation. Only model computations using the Nebraska Mesonet (Mesonet) weather data and with ground data in the atmospheric corrections for the thermal infrared imagery were used for this purpose. The justification for this is described later in the Discussion section. Crop coefficients were also computed with forecasted peak and end SAVI values to assess the performance for real-time functionality.

Modeled instantaneous energy flux components (from the TSEB) and daily ET (from the TSEB, K_{cbrf}, and hybrid method) were compared with eddy covariance measurements. The primary metrics of model performance were the root mean squared error (RMSE) and mean bias error (MBE) of the model as compared with the eddy covariance data. Nine-pixel average values from the modeled output were used in most of these comparisons (based on I. Campos, personal communication). The nine pixels were in the vicinity south of each flux tower (tower locations for this purpose were obtained from Google Earth). Nine pixels represented an area of 0.81 ha. The pixels were selected south of the towers to correspond approximately with the prevailing wind direction. Because of missing data in the Landsat 7 images, the distance south of each tower varied, so the same nine pixels were used for each tower for all comparisons herein. The center pixel was the pixel immediately south of the flux tower (about 30 m away) for CSP1, the third pixel south of the tower and (perhaps unnecessarily) about one pixel west (about 90 m away) for CSP2, and about 240 m south of the tower for CSP3. In comparing the total season ET, only one pixel was used for each eddy covariance tower.

Results

Experimental Conditions

The 2012 growing season was particularly dry at the research site. Total precipitation for May through October in 2012 for the nearby (NCEI, 2017) National Weather Service Global Climatic Data Network Mead 6 S site was about 310 mm. This was considerably below the 1981-2010 normal of about 540 mm (NCEI 2018). Precipitation amounts for May through October in 2011 and 2013 were similar to the normal, i.e., about 600 and 540 mm, respectively. Total May-October eddy covariance ET for CSP1 ranged from about 715 mm in 2011 to 779 mm in 2012. The May-October ET for CSP2 similarly ranged from about 700 mm in 2011 and 2013 to 752 mm in 2012. For CSP 3, the May-October ET was about 552 mm in 2012 and 573 mm in 2011. The average May-October ET was about 4 mm d^{-1} for the irrigated locations (CSP1 and CSP2) and about 3 mm d^{-1} for the rainfed location (CSP3).

Two-Source Energy Balance Model

Plots of the modeled instantaneous energy fluxes versus the measured fluxes are presented in figure 3 for an example set of conditions. The conditions were thermal infrared corrections with local ground data, using the Mesonet weather data, and with peak LAI and crop height used in the late season. The modeled crop heights appeared to be biased low on average, as compared to observations in the CSP fields. Both PM and PT approximations were used in computing the fluxes presented in figure 3.

A summary of the model fit statistics for the various TSEB model conditions as compared with eddy covariance data is presented in table 4. The RMSE for ET ranged from

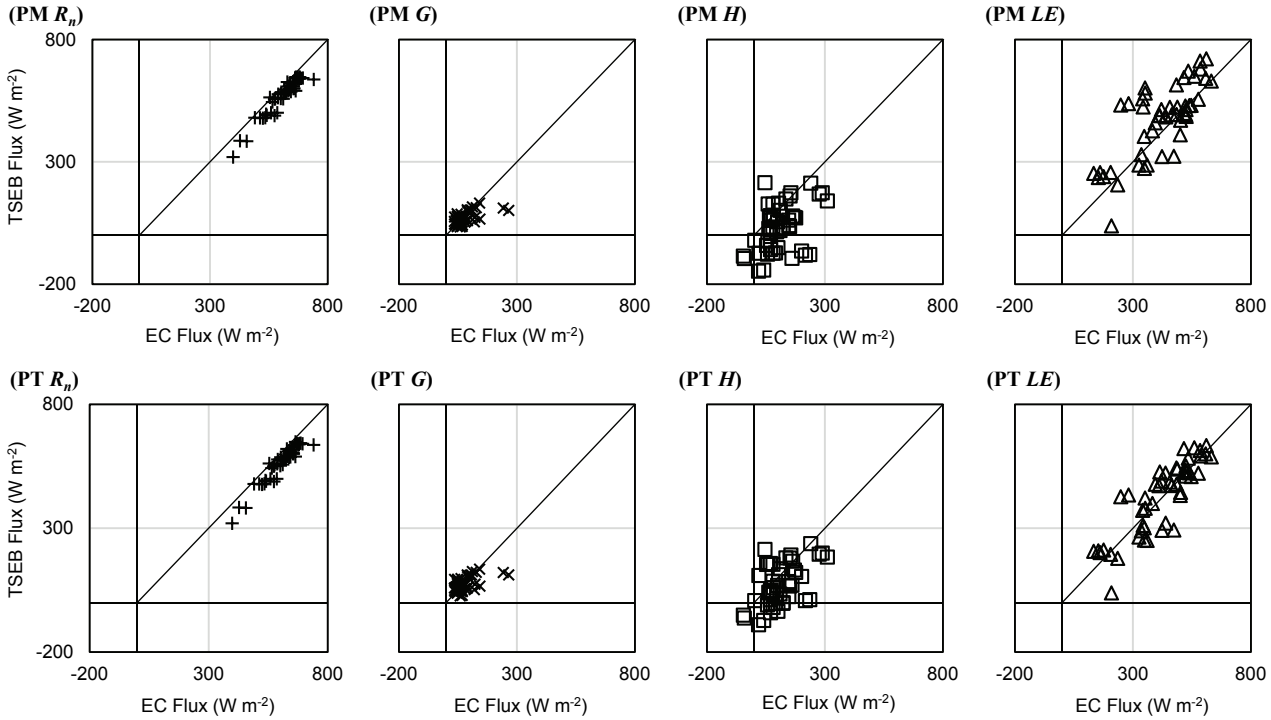

Figure 3. Comparison of two-source energy balance (TSEB) modeled energy fluxes with measured fluxes for Penman-Monteith (PM) and Priestly-Taylor (PT) approximations. The solid lines are unity. The TSEB was run using peak LAI in September and October and peak crop height up to the current image throughout the season (practically applied after early July). Mesonet weather data were used and ground data were used in thermal infrared imagery corrections. R_n, G, H, and LE are net radiation, soil heat flux, sensible heat flux, and latent heat flux, respectively.

Table 4. Model performance statistics summary for two-source model compared with closure-forced eddy covariance data (n = 50).

			Mean Biased Error (RMSE in parentheses)[c]				
Data Source	Method[a]	Senescence LAI and h_c[b]	R_n (W m^{-2})	G (W m^{-2})	H (W m^{-2})	LE (W m^{-2})	ET (mm d^{-1})
Mesonet, with ground data for thermal infrared correction	PM	Current	-34.5 (40.1)	-5.0 (37.7)	-124.6 (176.5)	95.1 (157.4)	1.4 (2.3)
		Peak	-38.6 (44.4)	-9.1 (37.2)	-78.2 (120.4)	48.6 (110.3)	0.8 (1.7)
	PT	Current	-37.8 (42.6)	-0.4 (38.5)	-70.9 (113.1)	33.5 (83.5)	0.5 (1.2)
		Peak	-40.9 (46.1)	-5.4 (37.4)	-39.8 (87.3)	4.3 (74.6)	0.1 (1.1)
Mesonet, without ground data for thermal infrared correction	PM	Current	-33.8 (39.5)	-4.9 (36.7)	-124.2 (174.8)	95.3 (159.3)	1.4 (2.3)
		Peak	-37.9 (43.9)	-8.8 (36.2)	-77.9 (119.1)	48.9 (114.1)	0.8 (1.8)
	PT	Current	-37.1 (42.0)	-0.2 (37.2)	-69.3 (106.8)	32.4 (81.1)	0.5 (1.1)
		Peak	-40.2 (45.5)	-5.2 (36.1)	-38.3 (79.3)	3.3 (72.0)	0.1 (1.0)
Flux tower, with ground data for thermal infrared correction	PM	Current	10.4 (26.5)	5.8 (37.6)	-87.5 (137.2)	92.1 (138.6)	1.3 (2.0)
		Peak	6.0 (25.1)	1.1 (35.6)	-50.5 (90.9)	55.4 (97.1)	0.8 (1.5)
	PT	Current	9.1 (25.8)	5.9 (38.4)	-66.4 (109.2)	69.6 (104.0)	0.9 (1.4)
		Peak	5.3 (25.3)	0.7 (35.8)	-35.3 (78.4)	39.9 (80.4)	0.5 (1.1)
Flux tower, without ground data for thermal infrared correction	PM	Current	11.2 (26.5)	5.7 (36.5)	-86.8 (134.6)	92.4 (138.6)	1.3 (1.9)
		Peak	6.8 (25.2)	1.1 (34.5)	-50.2 (88.1)	55.8 (98.4)	0.8 (1.5)
	PT	Current	9.8 (25.6)	6.0 (37.3)	-65.5 (104.4)	69.4 (101.5)	0.9 (1.3)
		Peak	6.0 (25.1)	0.9 (34.6)	-34.5 (71.8)	39.7 (77.3)	0.6 (1.0)
Mean eddy covariance values			606.7	76.9	110.3	419.6	5.9

[a] LE_c approximation method: PM is Penman-Monteith, and PT is Priestly-Taylor.

[b] Method for computing leaf area index and crop height during senescence: "Current" uses values computed for the current date, and "Peak" uses the maximum of current and previous values.

[c] Here, R_n, G, H, and LE are instantaneous net radiation, soil heat flux, sensible heat flux, and latent heat flux, respectively. The ET is scaled daily ET.

1.0 to 2.3 mm d^{-1}, with MBE ranging from 0.1 to 1.4 mm d^{-1}. Generally, the time-scaled ET in table 4 had similar MBE (in relation to the mean measured values), as did the instantaneous LE. Therefore, we did not suspect the scaling method to be introducing notable bias (eq. 5). However, to avoid introducing additional bias into the water balance model, we computed scaling factors (C_{ET}) to adjust for this discrepancy as $C_{ET}ET_d$ as used for a different scaling method by Gonzalez-Dugo et al. (2009), who cite Anderson et al. (1997), and who were referred to by I. Campos (personal communication). In computing the scaling factors, we split the data into calibration and validation sets. We anticipated that both year and location (because of the presence of both rainfed and irrigation conditions) would affect results. Therefore, we randomly selected one site from each year, also constrained to include only one year for each site for the validation dataset. The validation set included 2011 CSP3, 2012 CSP1, and 2013 CSP2. Note that all of the validation

Table 5. Two-source model performance statistics for validation dataset (n = 17) and computed weighting factors (W; Neale et al., 2012) from calibration dataset (n = 33) for use in incorporating two-source energy balance evapotranspiration into the water balance model.

			Without ET Scaling[c]		With ET Scaling[c]	
Data Source	TIR Correction[a]	TSEB Method[b]	MBE (RMSE) (mm d^{-1})	W (-)	MBE (RMSE) (mm d^{-1})	W (-)
Nebraska Mesonet	With ground data	PM	0.80 (1.88)	0.39	0.09 (1.49)	0.44
		PT	0.10 (1.20)	0.56	0.04 (1.18)	0.57
	Without ground data	PM	0.98 (1.82)	0.37	0.25 (1.36)	0.42
		PT	0.19 (0.98)	0.59	0.13 (0.96)	0.60
Flux towers	With ground data	PM	0.99 (1.63)	0.47	0.26 (1.19)	0.50
		PT	0.63 (1.19)	0.59	0.19 (0.94)	0.62
	Without ground data	PM	1.07 (1.57)	0.45	0.33 (1.10)	0.49
		PT	0.71 (1.04)	0.61	0.26 (0.75)	0.64

[a] Thermal infrared atmospheric corrections with and without including local ground data from the Nebraska Mesonet weather station.
[b] TSEB LE_c approximation method: PM = Penman-Monteith, and PT = Priestly-Taylor.
[c] "ET Scaling" indicates whether or not the TSEB evapotranspiration scaling factor was included.

samples were maize. The other six site-year combinations were included in the calibration set. The total number of samples in the validation set was 17, with 33 in the calibration set.

The C_{ET} values were computed using the TSEB computations with crop height and LAI maintained at peak during senescence, as described earlier. The C_{ET} values were similar for both thermal infrared correction methods; therefore, an average of the two was used in subsequent analysis. However, the C_{ET} values were notably different for PM and PT. The factors were also different if Mesonet or flux tower weather data were used. The C_{ET} values for the PM method were 0.89 for all model conditions. The C_{ET} values for PT were 0.93 and 0.99 using the flux tower and Mesonet weather data, respectively. The MBE and RMSE for daily ET with and without scaling factors (C_{ET}) are presented in table 5 for the validation data. All results in table 5 include the peak crop height and LAI methodologies.

Weights (W, eq. 7) for statistical interpolation (Neale et al., 2012, who cite Daley, 1991) were computed for PM and PT using a variety of TSEB modeling conditions (table 5). The same calibration set as described for the ET scaling computations was maintained for computing W. In all cases, the PT approximation resulted in larger W. The W value represents the ratio of water balance ET error variance over the sum of water balance and TSEB error variance (Neale et al., 2012). The W value ranges from 0 (water balance ET perfectly fit to measured values) to 1 (TSEB perfectly fit to measured values). A value of 0.5 means that the TSEB and water balance ET have the same error variance, although not necessarily identically modeled values. The PT approximation resulted in W values in the 0.56 to 0.64 range, while the PM W was 0.37 to 0.50.

Reflectance-Based Crop Coefficients

One major modification to the SETMI water balance model was the inclusion of a K_{cb} methodology after Campos et al. (2017). Plots of computed K_{cb} curves and individual image K_{cbrf} values for each site and year, following Campos et al. (2017) as modified by us, are presented in figure 4. The K_{cb} plots were presented for a single pixel in the center of the nine pixels used in each field for model comparisons. The limit (or maximum date) for which a peak SAVI value could be considered stage 1 (fig. 2) was reached for at least some pixel-year(s) in the analysis, causing such

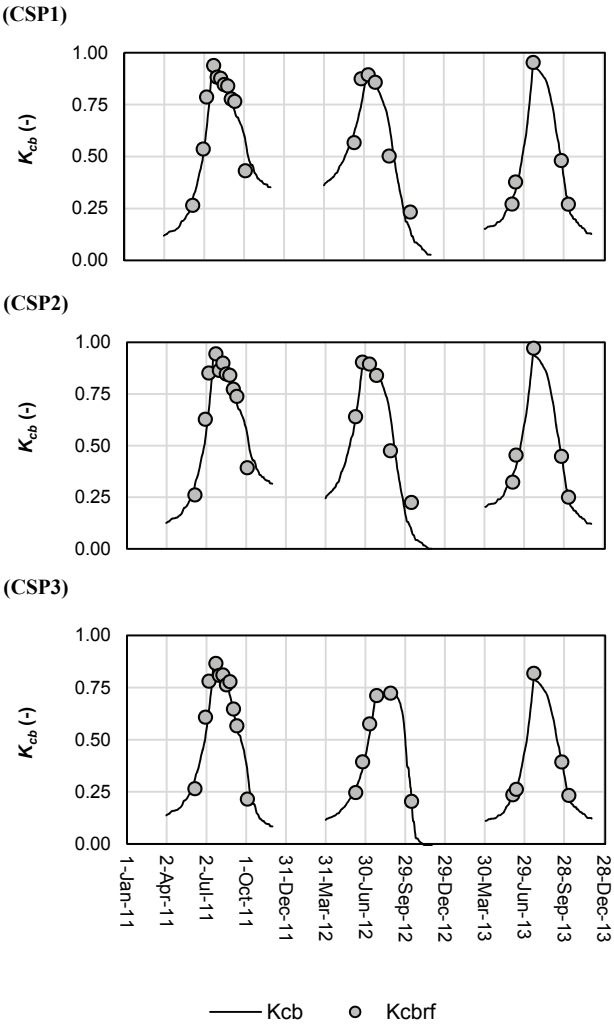

Figure 4. Plots of SETMI modeled K_{cbrf} with computed K_{cb} curve following Campos et al. (2017) as modified by us for one pixel in each of the three flux tower fields. The Mesonet data were used to compute these K_{cb} values.

pixel-year(s) to be considered as stage 2. In figure 4, the 2012 K_{cb} for CSP3 was included in this constraint; the other eight pixel-years in this figure did not reach this constraint.

Because the intent of the current study was to validate the model for real-time irrigation management, an example plot of K_{cb} progression with various numbers of input images for a single maize pixel in CSP1 in 2011 is provided in figure 5.

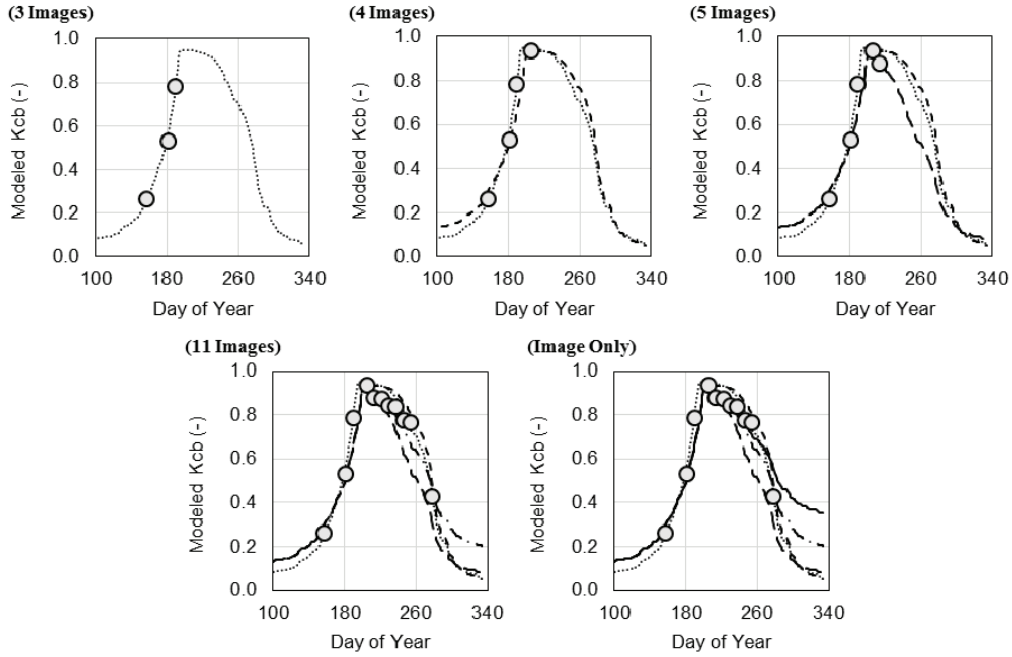

Figure 5. Plot of progression of SETMI-modeled maize K_{cb} for one pixel in CSP1 in 2011 using only images (Image Only) and in real-time mode with a projected end SAVI on day-of-year 304. A forecasted peak SAVI was also used in the first plot (3 Images). The K_{cbrf} points are the actual pixel values. A total of 11 images were included in 2011. The Mesonet data were used to compute these K_{cb} values.

The first four plots are a demonstration of real-time operation with forecasted peak and/or ending SAVI values. The first of these plots includes the first three early-season images before peak, as listed in table 3. In this case, a forecasted peak SAVI of 0.686 ($K_{cbrf} \approx 0.95$) was applied and allowed to occur at any time up to day-of-year 232. A projected end SAVI of 0.099 ($K_{cbrf} \approx 0.12$) was also added on day-of-year 304. The next K_{cb} curve in figure 5 includes four input images, one of which was the peak, so the forecasted peak was no longer used, but this plot still includes the projected end SAVI. The next two curves include the first 5 images and all 11 images, still with the projected end SAVI. The final plot in figure 5 includes all 11 images from 2011, with no projected end SAVI.

Water Balance and Hybrid Models

In validating the K_{cbrf} and hybrid model ET, herein referred to as water balance ET, the full set of input imagery listed in table 3 was used, as opposed to the real-time methodology as in figure 5. As both the PM and PT methods in the TSEB were of interest, water balance ET was computed by incorporating TSEB ET using both methods. However, TSEB ET was only computed for the conditions that were stated above for developing figure 3. Water balance results are presented for the validation dataset only. The water balance was computed without incorporating TSEB ET for the calibration dataset to compute the W factors presented in table 5. Two resulting plots of TSEB and water balance ET using the PM and PT approaches as just described, as compared with eddy covariance ET, are presented in figure 6 for the validation dataset (n = 17). A similar figure is presented in figure 7 in which ET computed over the period of May through October was included for only one pixel in each of the site-years in the validation set. All ET values in figure 7 were seven-day running averages, starting on May 1 (i.e., including the last six days of April in the average) and ending on October 31. A visible lobe of underestimated data is apparent in figure 7 for the hybrid ET using the PM and PT methods in the TSEB. These data were primarily following incorporation of TSEB ET from June 11, 2013. When this date was excluded from the TSEB ET incorporation, the "Excluding June 11, 2013" graph resulted.

Model fit statistics were computed for the water balance by comparing the nine-pixel average ET with the eddy covariance ET for the same periods that were used in the TSEB evaluation. The fit statistics were also computed for a single pixel in each of the three site-years in the validation set for the seven-day running averages of ET for May through October. The model fit statistics were computed for ET with and without TSEB ET incorporation. The combined results are presented in table 6. For demonstration purposes, model statistics are also presented excluding June 11, 2013, for CSP2 from both the validation dataset and the TSEB ET incorporation.

Discussion

Two-Source Energy Balance Model

The underestimation of R_n when using the Mesonet data is observable in figure 3 and was presumably caused by the low solar radiation data. There is notable scatter in H and LE as compared with the results of Neale et al. (2012) using the TSEB with the PT approximation over cotton. One possible cause could be that the atmospheric corrections for some of the thermal infrared imagery were perhaps not accurate in our study. We did not exclude imagery on the basis of thermal infrared correction parameters. Therefore, some correction parameters may have been such that they resulted in

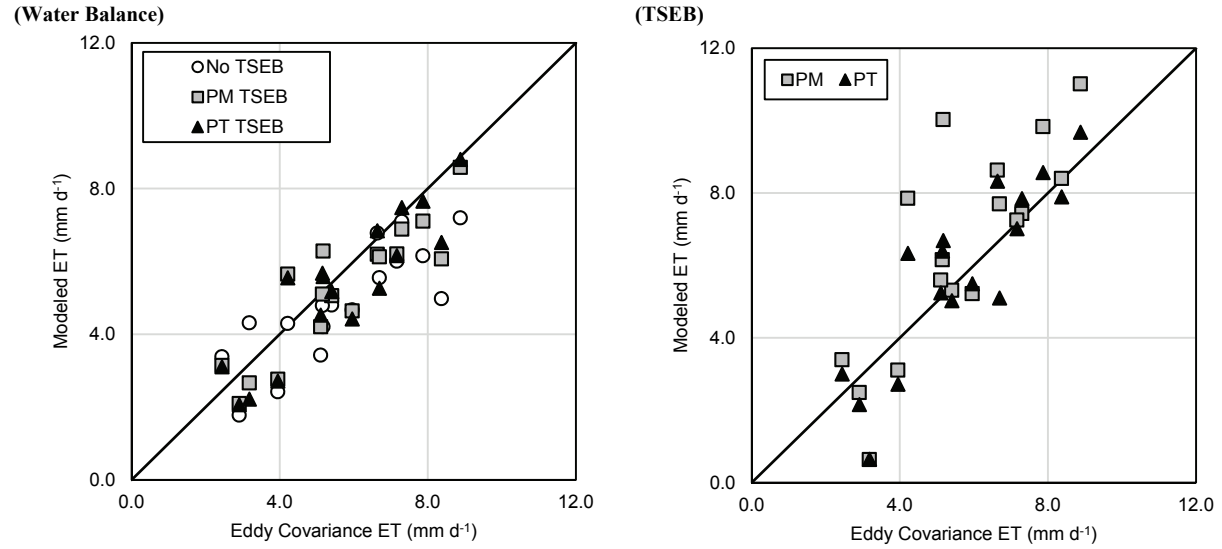

Figure 6. Plot of SETMI water balance (left) and TSEB (right) modeled ET with eddy covariance measured ET for the validation data set (n = 17). Solid lines are unity. Only the Mesonet weather data were used here. Ground data were used in thermal infrared image corrections. The TSEB ET was scaled to reduce bias. PM and PT are Penman-Monteith and Priestly-Taylor approximations in the TSEB, respectively. "TSEB" and "No TSEB" are with and without incorporating TSEB ET, respectively.

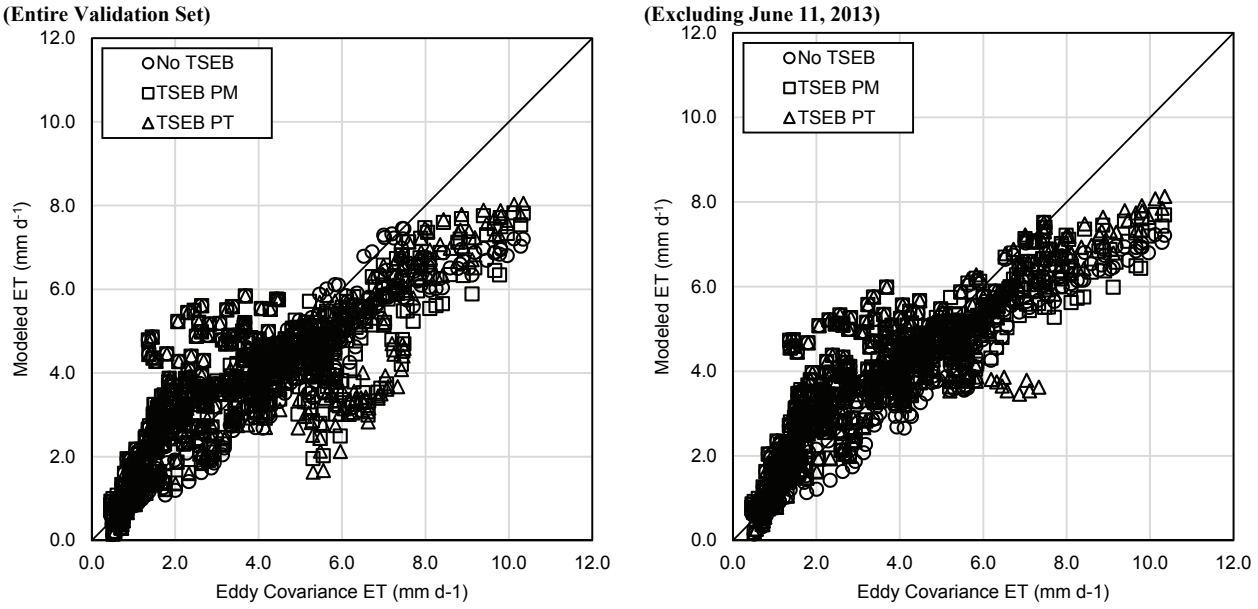

Figure 7. Plot of SETMI water balance modeled seven-day running average ET with seven-day running average eddy covariance ET for the validation dataset for May through October. The "entire validation set" graph includes incorporated TSEB ET for all 17 validation images. "Excluding June 11, 2013" does not include TSEB ET from that date. The solid line is unity. Only the Mesonet weather data were used here. Ground data were used in thermal infrared image corrections. The TSEB ET was scaled to reduce bias. PM and PT are Penman-Monteith and Priestly-Taylor approximations in the TSEB, respectively. "TSEB" and "No TSEB" are with and without incorporating TSEB ET, respectively.

overcorrection. We assumed that the imagery was adequate based on the apparent absence of clouds and cloud shadows over necessary areas of the study. There is a cluster of six *LE* points in the PM plot in figure 3 that appear to be notably more overestimated than others. These points were all from the two irrigated fields and occurred on June 30, 2011, on June 8, 2012, and on August 27, 2012. This cluster was not clearly apparent in the PT plot.

Many of the RMSE and MBE values for the modeled R_n, *H*, and *LE* fluxes reported in table 4 were greater in magnitude than those reported by Neale et al. (2012), who used the PT method. They reported RMSE values of 46 and 41 W m^{-2} for *H* and *LE*, respectively. Our RMSE values were in the range of 72 to 120 W m^{-2} for *H* when peak crop height and LAI were included. We also found RMSE for *LE* to be about 72 to 114 W m^{-2} under these same model conditions. One reason for the difference could be that Neale et al. (2012) ran the model as part of a much more detailed exper-

Table 6. Model performance statistics for the validation dataset (nine-pixel) and May through October seven-day running averages (one-pixel) for the validation site-years as compared with eddy covariance seven-day average ET.

		MBE (mm d^{-1}, RMSE in parentheses) for Different Water Balance Options[a]					
		Entire Validation Set (n = 17)			Excluding June 11, 2013 (n = 16)[b]		
Data Source	Dataset	TSEB PM	TSEB PT	No TSEB	TSEB PM	TSEB PT	No TSEB
Mesonet	Validation	-0.45 (0.98)	-0.39 (0.95)	-0.86 (1.37)	-0.29 (1.02)	-0.22 (0.99)	-0.86 (1.37)
	May-October	-0.12 (1.29)	-0.14 (1.33)	-0.06 (1.12)	0.07 (1.08)	0.05 (1.09)	-0.06 (1.12)
Flux tower	Validation	-0.28 (0.98)	-0.22 (0.84)	-0.88 (1.51)	-0.16 (1.03)	-0.08 (0.92)	-0.88 (1.51)
	May-October	-0.03 (1.25)	-0.05 (1.28)	-0.01 (1.13)	0.14 (1.08)	0.12 (1.08)	-0.01 (1.13)

[a] "TSEB" is with TSEB ET incorporation, and "No TSEB" is without doing so. PM and PT are Penman-Monteith and Priestly-Taylor approximations in the TSEB. The water balance was computed using the Mesonet data only, with ET bias scaling and with ground data for thermal infrared corrections in the TSEB ET.

[b] The TSEB ET for CSP2 from June 11, 2013, was not incorporated into the model, and validation statistics were not computed for that date. The statistics under this heading are for demonstration purposes only.

iment using high-resolution multispectral and thermal infrared imagery from the Utah State University airborne system with more frequent data inputs. Their modeling period included the first half of the growing season, with multiple remote sensing inputs during the vegetative stage of growth and full cover periods. The current study included more images but at generally lower temporal frequency. This study also included late-season images and different crops than Neale et al. (2012).

The RMSE values for R_n in table 4 were similar to Colaizzi et al. (2012b), who found the RMSE to be 28 W m^{-2} over many measurements and times of day. Our RMSE was about 25 to 46 W m^{-2}. Colaizzi et al. (2012b) used the PM method. Note that R_n was better fit when the flux tower data were used.

We modeled H with somewhat better accuracy when the flux tower data were used. The LE estimates had similar to greater variability as compared to Colaizzi et al. (2012b), who used a PM formulation of the TSEB. Our RMSE values ranged from about 72 to 114 W m^{-2}, when peak LAI and crop height were used, as compared to about 67 W m^{-2} for Colaizzi et al. (2012b). Our MBE values for both LE and R_n were of greater magnitude, in general, than those reported by Colaizzi et al. (2012b).

Modeled LE was comparable or better (in the case of PT) when the Mesonet data were used as model input. However, this was at the expense of R_n bias. Modeled LE was overestimated by PM in all cases, as it was for PT when the flux tower data were used. Because the flux tower data are not readily available in real-time, using the Mesonet data may be most reasonable in real-time applications with current model parameterizations. The model performed similarly regardless of the thermal infrared correction method.

Daily ET was overestimated for all model options (table 4). The PM ET was greater than the PT ET in all cases in table 4. Colaizzi et al. (2014) found that the PT method resulted in an underestimation of ET while the PM did not for measurements at 11:15 a.m. (comparable with the Landsat overpass times in our study). Colaizzi et al. (2014) used infrared thermometers rather than satellite imagery, and their study was over cotton in Texas. They found that PT ET had a larger RMSE than PM ET, which was the opposite of our results. One cause of the difference could be that our ENREC site may be more humid than their site.

The computed C_{ET} values in the 0.9 range were comparable to the results of Chavez et al. (2008), who found that this type of temporal scaling method was biased high, with MBEs in the 9% to 24% range in their study of maize and soybean, although they forced EC closure differently than we did for this part of their analysis. In all conditions, RMSE improved with ET scaling (table 5), which followed expectations.

The W results in table 5 reveal that the PM ET had greater error variance than the PT ET. This follows the results in table 4. It is clear that further improvements may be needed in the model. The W values in table 5 for both models were much smaller than the value of 0.78 for the PT method reported by Geli (2012) for maize and soybean in Iowa.

Overall, the TSEB performed well when compared with the eddy covariance data. The PM and PT methods both resulted in relatively low bias compared to measurements. It appears that the PT method in this version of SETMI may be the better choice for our location and for the crop conditions in this study. However, the performance of the PM method was not dramatically different. We anticipate that the PM method is more broadly applicable than the PT method, particularly when applied in more arid conditions than in the present study (e.g., Colaizzi et al., 2014; D. L. Martin, personal communication).

Reflectance-Based Crop Coefficients

Overall, the K_{cb} relationships in figure 4 are reasonable, although it is clear that the performance was better when more images were available (see 2011 as compared with 2012 and 2013). The K_{cb} curves tend to show a cusp at peak values, which may be attributed to a lack of images in the middle of the growing season in 2012 and 2013. However, this behavior appears even in 2011 when multiple mid-season images were available (compared to other years) and appears to follow the K_{cbrf} values well.

The K_{cb} curves in figure 5 rapidly approach the curve with all 11 images. It is clear that there was some overestimation with three images and four images, but with five images there was a drop below the eventual level. This demonstrates the dependence of the model on input imagery near the peak of the season. The methodology still presents benefits over traditional time-only-based K_{cb} curves, as have been identified by others (e.g., Hunsaker et al., 2005). The real-time method also requires few inputs beyond the reflectance imagery.

Hybrid Methodology

The water balance appeared to have less negative bias after incorporation (fig. 6). The lobe of underestimated ET on the high end of the graph in figure 7 is mostly data points from the summer of 2012. As mentioned earlier, the 2012

growing season was a particularly dry year. While it would have been possible to calibrate the root zone depth for that year (Campos et al., 2017; Allen et al., 2015; I. Campos, personal communication), such an effort was not consistent with the objectives of this study. The considerable lobe of underestimated ET in the "entire validation set" graph in figure 7 occurred as a result of incorporating TSEB ET from June 11, 2013, which was low. Excluding this date from the hybrid model resulted in better model performance. However, excluding that date is not justifiable, statistically speaking, and was done only for demonstration purposes. Noting these exceptions, the water balance model appeared to have performed well, considering that it was not calibrated to the site, beyond computing W and C_{ET}, and acknowledging that the K_{cbrf} relationships used here were developed using data from the same flux towers (Campos et al., 2017). The model performance may be improved by modifying the wet soil evaporation term (e.g., Torres and Calera, 2010; I. Campos, personal communication).

Incorporation of TSEB ET for both the PM and PT methods resulted in less bias and less RMSE than the unaided water balance if only the validation dataset was considered. However, for the May through October analysis, the hybrid methodology did not result in model improvement unless June 11, 2013, was dropped from the analysis and TSEB ET incorporation (table 6). In this case, the model performance was not always improved, and when it was improved it was not by much. In terms of the MBE and RMSE values in table 6 for the three included pixels (including the seven-day averaging), the PM and PT methods performed quite similarly. The reduced bias in the validation dataset following TSEB ET incorporation supports the hypothesis that the hybrid model would perform better than the K_{cbrf} (or TSEB) alone. However, the May through October analysis suggests otherwise. It is evident that, without further improvements, the water balance may be best run at this location without the hybrid methodology.

The low availability of satellite imagery may have caused some of the poor model performance in this study. Only Landsat 7 was operational in 2012, and imagery was limited due to cloud cover in 2013. This highlights the importance of frequent image inputs for this model. Future work should include additional data sources such as aerial imagery, including unmanned aircraft. Gowda et al. (2007) discussed that a challenge with using Landsat imagery for irrigation management is the temporal availability of data, mentioning both the temporal frequency of imagery and the time between data collection and availability. The former is of particular concern in eastern Nebraska and in other locations, where frequent cloud cover limits the number of usable satellite images during the growing season. We expect that the hybrid model is less sensitive to the time between image acquisition and availability (within reason).

We feel that the water balance model is adequately parameterized for use as an irrigation scheduling tool at the research location. However, the hybrid methodology will require additional development. In irrigation management, the model could be applied with forecasted ET_r, which is not discussed here. The use of satellite imagery or aerial imagery in the model allows computation of a spatial water balance that may be used for irrigation scheduling, including VRI management.

Summary and Conclusions

A hybrid remote sensing ET and soil water balance model was evaluated for use in irrigation management. The model included ET computed using a version of the TSEB of Norman et al. (1995) and K_{cbrf} values. The TSEB energy fluxes were compared with eddy covariance fluxes for three sites within the study area. The Priestly-Taylor (PT) approximation method performed better than the Penman-Monteith (PM) method in modeling ET at the study location. This is contrary to the results of Colaizzi et al. (2014), who found the opposite in northern Texas. We acknowledge the interdependence of the R_n computations in the temperature partitioning (D. L. Martin, personal communication), but we do not expect that the SETMI model is formulated in a way that favors the PT method. The similar results for R_n and G between the two methods, in contrast to H and LE, suggest that the primary differences between PT and PM reside in H and LE. Further work at other sites is recommended to identify the conditions under which the PT or PM method may perform best. We expect the PM method to be broadly applicable (D. L. Martin, personal communication). The inclusion of input peak past crop height throughout the season and LAI in September and October improved the model performance in general.

The K_{cbrf} method of Campos et al. (2017) as modified by us appears to have performed well for years with many shortwave reflectance images (2011) and for years with few images (2012 and 2013). The methods implemented to compute the K_{cb} in real time, including adding forecasted peak and ending SAVI values, produced reasonable results. The robustness of the model for irrigation scheduling should be tested over a wider range of climate conditions.

Water balance modeled ET generally compared well with the eddy covariance data for the validation dataset. However, the model computed water stress that was not represented in the eddy covariance data. Inadequate root zone depth may have been a cause. This suggests that a single modeled root zone depth may not be adequate for all years or conditions. However, this may be less problematic if the model is used for irrigation scheduling. Improved parameterization of the water balance soil evaporation model may also help address some of the model bias. Poor temporal frequency of satellite imagery because of cloud cover and satellite operation in 2012 and 2013 was identified as a challenge in applying this methodology. Future work should focus on model testing and further parameterization of the model in other locations and the use of aerial imagery to improve the frequency of remote sensing inputs.

Acknowledgements

This work was supported by the USDA National Institute of Food and Agriculture (Hatch Project 1009760) and Agriculture Food and Research Initiative grant (Award No. 2017-67021-26249), the University of Nebraska-Lincoln Agricultural Research Division, the Robert B. Daugherty Water for

Food Global Institute at the University of Nebraska, and the Department of Biological Systems Engineering at the University of Nebraska-Lincoln. Barker received some support through a University of Nebraska Presidential Graduate Fellowship. The Carbon Sequestration Project sites support has included the U.S. Department of Energy, NASA, and the University of Nebraska-Lincoln Agricultural Research Division (see Campos et al., 2017; http://csp.unl.edu/Public/acknowledgements.htm). We thank Dr. Hatim Geli and Dr. Clayton Lewis, formerly of the Utah State University Remote Sensing Services Laboratory, who provided the initial computer code for the SETMI model and additional help; Dr. Martha Anderson and Dr. William Kustas of the USDA-ARS Hydrology and Remote Sensing Laboratory in Beltsville, Maryland, and Dr. Héctor Nieto Solana of IRTA (Food and Agriculture Research and Technology) in Barcelona, Spain, for their assistance and access to code for the TSEB model. Dr. Paul Colaizzi of the USDA-ARS Conservation and Production Research Laboratory in Bushland, Texas, provided assistance with the PM approximation and other TSEB formulations. Dr. Richard Allen of the University of Idaho provided insight on the wind speed adjustments. The High Plains Regional Climate Center provided necessary weather data for the Memphis 5N and Mead 6 S stations. We also thank Mr. Mark Schroeder, Director of the Agricultural Research and Development Center at ENREC, and Mr. Todd Shimelfenig, Research Manager of the University of Nebraska Carbon Sequestration Project, who provided crop management records; Mr. Shimelfenig provided clarification on irrigation records. “Funding for AmeriFlux [core site] data resources was provided by the U.S. Department of Energy’s Office of Science” (http://ameriflux.lbl.gov/data/data-policy/). Landsat data, including surface reflectance products were obtained from the U.S. Geological Survey. Mr. Christian Uwineza assisted in obtaining thermal infrared atmospheric correction parameters. Mr. Raoni W. D. Bosquilia also provided assistance and insight in the thermal infrared corrections. Dr. Isidro Campos of the University of Castilla-La Mancha, formally at the Daugherty Water for Food Global Institute, provided assistance with the water balance model. We thank Ms. Ronica Stromberg and Mr. Sandeep Bhatti for their grammatical reviews and Dr. Trenton Franz, Dr. Derrel Martin, and Dr. William Kranz for their critical reviews of the manuscript. We also thank the two anonymous reviewers who provided input to the version of the manuscript presented at the 2015 joint ASABE and Irrigation Association Irrigation Symposium in Long Beach, California, and the three anonymous reviewers who provided valuable reviews for the present article.

REFERENCES

Allen, R. G., Kilic, A., Suyker, A., & Okalebo, J. (2015). Fitting measured evapotranspiration data to the FAO-56 dual crop coefficient method. ASABE Paper No. 152143520. St. Joseph, MI: ASABE. https://doi.org/10.13031/irrig.20152143520.

Allen, R. G., Pereira, L. S., Raes, D., & Smith, M. (1998). Crop evapotranspiration: Guidelines for computing crop water requirements. Irrigation and Drainage Paper 56. Rome, Italy: United Nations FAO.

Allen, R. G., Tasumi, M., Morse, A., Trezza, R., Wright, J. L., Bastiaanssen, W., Kramber, W., Lorite, I., & Robinson, C. W. (2007a). Satellite-based energy balance for mapping evpotranspiration with internalized calibration (METRIC) – Application. *J. Irrig. Drain. Eng., 133*(4), 395-406. https://doi.org/10.1061/(ASCE)0733-9437(2007)133:4(395)

Allen, R. G., & Wright, J. L. (1997). Translating wind measurements from weather stations to agricultural crops. *J. Hydrol. Eng., 2*(1), 26-35. https://doi.org/10.1061/(ASCE)1084-0699(1997)2:1(26)

Allen, R. G., Wright, J. L., Pruitt, W. O., Pereira, L. S., & Jensen, M. E. (2007b). Chapter 8: Water requirements. In G. J. Hoffman, R. G. Evans, M. E. Jensen, D. L. Martin, & R. L. Elliott (Eds.), *Design and operation of farm irrigation systems* (2nd ed., pp. 208-288). St. Joseph, MI: ASABE.

Anderson, M. C., Neale, C. M. U., Li, F., Norman, J. M., Kustas, W. P., Jayanthi, H., & Chavez, J. L. (2004). Upscaling ground observations of vegetation water content, canopy height, and leaf area index during SMEX02 using aircraft and Landsat imagery. *Remote Sens. Environ., 92*(4), 447-464. https://doi.org/10.1016/j.rse.2004.03.019

Anderson, M. D., Norman, J. M., Diak, G. R., Kustas, W. P., & Mecikalski, J. R. (1997). A two-source time-integrated model for estimating surface fluxes using thermal infrared remote sensing. *Remote Sens. Environ., 60*(2), 195-216. https://doi.org/10.1016/S0034-4257(96)00215-5

ASCE (2005). ASCE standardized reference evapotranspiration equation. Reston, VA ASCE Environmental and Water Resources Institute. Retrieved from https://www.kimberly.uidaho.edu/water/asceewri/ascestzdetmain2005.pdf

Barker, J. B., Heeren, D. M., Neale, C. M. U., & Rudnick, D. R. (2018). Evaluation of variable-rate irrigation using a remote-sensing-based model. *Agric. Water Mgmt.,* (https://doi.org/10.1016/j.agwat.2018.02.022).

Barsi, J. (2018). Atmospheric Correction Parameter Calculator. Washington, DC: National Aeronautic and Space Administration. Accessed March 2, 2018. Available at https://atmcorr.gsfc.nasa.gov

Barsi, J. A., Barker, J. L., & Schott, J. R. (2003). An atmospheric correction parameter calculator for a single thermal band earth-sensing instrument. *Proc. IEEE Intl. Geoscience and Remote Sensing Symposium (IGARSS 2003)* (vol. 5, pp. 3014-3016). Piscataway, NJ: IEEE. https://doi.org/10.1109/IGARSS.2003.1294665

Bausch, W. C. (1993). Soil background effects on reflectance-based crop coefficients for corn. *Remote Sens. Environ., 46*(2), 213-222. https://doi.org/10.1016/0034-4257(93)90096-g

Bausch, W. C., & Neale, C. M. U. (1987). Crop coefficients derived from reflected canopy radiation: A concept. *Trans. ASAE, 30*(3), 703-709. https://doi.org/10.13031/2013.30463

Brunsell, N. A., & Gillies, R. R. (2002). Incorporating surface emissivity into a thermal atmospheric correction. *Photogram. Eng. Remote Sens., 68*(12), 1263-1269.

Brutsaert, W. (1982). *Evaporation into the atmosphere: Theory, history, and applications*. Dordrecht, The Netherlands: D. Reidel.

Campbell, G. S., & Norman, J. M. (2012). *An introduction to environmental biophysics* (2 ed.). New York, NY: Springer.

Campos, I., Neale, C. M. U., Calera, A., Balbontin, C., & Gonzalez-Piqueras, J. (2010). Assessing satellite-based basal crop coefficients for irrigated grapes (*Vitis vinifera* L). *Agric. Water Mgmt., 98*(1), 45-54. https://doi.org/10.1016/j.agwat.2010.07.011

Campos, I., Neale, C. M. U., Suyker, A. E., Arkebauer, T. J., & Gonçalves, I. Z. (2017). Reflectance-based crop coefficients

redux: For operational evapotranspiration estimates in the age of high-producing hybrid varieties. *Agric. Water Mgmt., 187*, 140-153. https://doi.org/10.1016/j.agwat.2017.03.022

Chavez, J. L., Neale, C. M. U., Prueger, J. H., & Kustas, W. P. (2008). Daily evapotranspiration estimates from extrapolating instantaneous airborne remote sensing ET values. *Irrig. Sci., 27*(1), 67-81. https://doi.org/10.1007/s00271-008-0122-3

Choudhury, B. J., Ahmed, N. U., Idso, S. B., Reginato, R. J., & Daughtry, C. S. T. (1994). Relations between evaporation coefficients and vegetation indices studied by model simulations. *Remote Sens. Environ., 50*(1), 1-17. https://doi.org/10.1016/0034-4257(94)90090-6

Colaizzi, P. D., Agam, N., Tolk, J. A., Evett, S. R., Howell, T. A., Gowda, P. H., ... Anderson, M. C. (2014). Two-source energy balance model to calculate E, T, and ET: Comparison of Priestley-Taylor and Penman-Monteith formulations and two time-scaling methods. *Trans. ASABE, 57*(2), 479-498. https://doi.org/10.13031/trans.57.10423

Colaizzi, P. D., Agam, N., Tolk, J. A., Evett, S. R., Howell, T. A., Sr., O'Shaughnessy, S. A., ... Anderson, M. C. (2016). Advances in a two-source energy balance model: Partitioning of evaporation and transpiration for cotton. *Trans. ASABE, 59*(1), 181-197. https://doi.org/10.13031/trans.59.11215

Colaizzi, P. D., Evett, S. R., Howell, T. A., Li, F., Kustas, W. P., & Anderson, M. C. (2012a). Radiation model for row crops: I. Geometric view factors and parameter optimization. *Agron. J., 104*(2), 225-240. https://doi.org/10.2134/agronj2011.0082

Colaizzi, P. D., Kustas, W. P., Anderson, M. C., Agam, N., Tolk, J. A., Evett, S. R., ... O'Shaughnessy, S. A. (2012b). Two-source energy balance model estimates of evapotranspiration using component and composite surface temperatures. *Adv. Water Resour., 50*, 134-151. https://doi.org/10.1016/j.advwatres.2012.06.004

COSMOS. (2017). Cosmic-ray soil moisture observing system: Level 1 data for Neb Field 3. Tucson, AZ: University of Arizona, Department of Hydrology and Atmospheric Sciences. Retrieved from http://cosmos.hwr.arizona.edu/Probes/StationDat/029/counts.txt

Daley, R. (1991). *Atmospheric data analysis*. Cambridge, UK: Cambridge University Press.

Geli, H. M. E. (2012). Modeling spatial surface energy fluxes of agricultural and riparian vegetation using remote sensing. PhD diss. Logan, UT: Utah State University. Retrieved from http://digitalcommons.usu.edu/etd/1165

Geli, H. M. E., Lewis, C. S., & Contributors. (2014). SETMI source code (ca. 5 November 2014). Logan, UT: Utah State University.

Geli, H. M. E., & Neale, C. M. U. (2012). Spatial evapotranspiration modelling interface (SETMI). In C. M. U. Neale & M. H. Cosh (Eds.), *Remote Sensing and Hydrology* (pp. 171-174). IAHS Proceedings and Reports 352. Wallingford, UK: International Association of Hydrological Sciences.

Gonzalez-Dugo, M. P., Neale, C. M. U., Mateos, L., Kustas, W. P., Prueger, J. H., Anderson, M. C., & Li, F. (2009). A comparison of operational remote sensing-based models for estimating crop evapotranspiration. *Agric. Forest Meteorol., 149*, 1843-1853. https://doi.org/10.1016/j.agrformet.2009.06.012

Gowda, P. H., Chavez, J. L., Colaizzi, P. D., Evett, S. R., Howell, T. A., & Tolk, J. A. (2007). Remote sensing based energy balance algorithms for mapping ET: Current status and future challenges. *Trans. ASABE, 50*(5), 1639-1644. https://doi.org/10.13031/2013.23964

Ham, J. M. (2005). Useful equations and tables in micrometeorology. In J. L. Hatfield & J. M. Baker (Eds.), *Micrometeorology in agricultural systems* (pp. 533-560). Madison, WI: ASA, CSSA, and SSSA.

Higgins, C. W., Kelley, J., Barr, C., & Hillyer, C. (2016). Determining the minimum management scale of a commercial variable-rate irrigation system. *Trans. ASABE, 59*(6), 1671-1680. https://doi.org/10.13031/trans.59.11767

Houborg, R., Anderson, M. C., Norman, J. M., Wilson, T., & Meyers, T. (2009). Intercomparison of a 'bottom-up' and 'top-down' modeling paradigm for estimating carbon and energy fluxes over a variety of vegetative regimes across the U.S. *Agric. Forest Meteorol., 149*(11), 1875-1895. https://doi.org/10.1016/j.agrformet.2009.06.014

Huete, A. R. (1988). A soil-adjusted vegetation index (SAVI). *Remote Sens. Environ., 25*(3), 295-309. https://doi.org/10.1016/0034-4257(88)90106-x

Hunsaker, D. J., Barnes, E. M., Clarke, T. R., Fitzgerald, G. J., & Pinter, P. J. (2005). Cotton irrigation scheduling using remotely sensed and FAO-56 basal crop coefficients. *Trans. ASAE, 48*(4), 1395-1407. https://doi.org/10.13031/2013.19197

Jensen, M. E. & Allen, R. G. (Eds.). (2016). *Evaporation, evapotranspiration, and irrigation water requirements.* 2nd Ed. ASCE Manuals and Reports on Engineering Practice No. 70. Reston, VA: ASCE Environmental and Water Resources Institute.

Kustas, W. P & Norman, J. M. (1997). A two-source approach for estimating turbulent fluxes using multiple-angle thermal infrared observations. *Water Resour. Res., 33*(6), 1495-1508. https://doi.org/10.1029/97WR00704

Kustas, W. P. & Norman, J. M. (1999). Evaluation of soil and vegetation heat flux predictions using a simple two-source model with radiometric termperatures for partial canopy cover. *Agric. Forest Meteorol., 94*(1), 13-29. https://doi.org/10.1016/S0168-1923(99)00005-2

Li, F. Q., Kustas, W. P., Prueger, J. H., Neale, C. M. U., & Jackson, T. J. (2005). Utility of remote sensing-based two-source energy balance model under low- and high-vegetation cover conditions. *J. Hydrometeorol., 6*(6), 878-891. https://doi.org/10.1175/jhm464.1

NCEI. (2017). Normals monthly station details. Asheville, NC: National Centers for Environmental Information. Retrieved from https://www.ncdc.noaa.gov/cdo-web/datasets/normal_mly/stations/GHCND:USC00255362/detail

NCEI. (2018). Data tools: 1981-2010 normals. Asheville, NC: National Centers for Environmental Information. Retrieved from http://www.ncdc.noaa.gov/cdo-web/datatools/normals

NDAWN. (2017). Corn growing degree days (GDD). Fargo, ND: North Dakota Agricultural Weather Network. Retrieved from https://ndawn.ndsu.nodak.edu/help-corn-growing-degree-days.html

Neale, C. M. U., Bausch, W. C., & Heermann, D. F. (1989). Development of reflectance-based crop coefficients for corn. *Trans. ASAE, 32*(6), 1891-1899. https://doi.org/10.13031/2013.31240

Neale, C. M. U., Geli, H. M. E., Kustas, W. P., Alfieri, J. G., Gowda, P. H., Evett, S. R., ... Howell, T. A. (2012). Soil water content estimation using a remote sensing based hybrid evapotranspiration modeling approach. *Adv. Water Resour., 50*, 152-161. https://doi.org/10.1016/j.advwatres.2012.10.008

Norman, J. M., Kustas, W. P., & Humes, K. S. (1995). A two-source approach for estimating soil and vegetation energy fluxes in observations of directional radiometric surface-temperature. *Agric. Forest Meteorol., 77*(3-4), 263-293. https://doi.org/10.1016/0168-1923(95)02265-y

O'Shaughnessy, S. A., Evett, S. R., & Colaizzi, P. D. (2015). Dynamic prescription maps for site-specific variable-rate irrigation of cotton. *Agric. Water Mgmt., 159*, 123-138. https://doi.org/10.1016/j.agwat.2015.06.001

Rondeaux, G., Steven, M., & Baret, F. (1996). Optimization of soil-adjusted vegetation indices. *Remote Sens. Environ., 55*(2), 95-

107. https://doi.org/10.1016/0034-4257(95)00186-7
Rouse, J. W., Haas, R. H., Schell, J. A., Deering, D. W., & Harlan, J. C. (1974). Monitoring the vernal advancement and retrogradation (greenwave effect) of natural vegetation. College Station, TX: Texas A&M University, Remote Sensing Center.
Soil Survey Staff (2016a). Soil Survey Geographic (SSURGO) database for Saunders County, Nebraska. Fort Worth, TX: USDA Natural Resources Conservation Service. Retrieved from https://websoilsurvey.sc.egov.usda.gov
Soil Survey Staff (2016b). Web Soil Survey. Washington, DC: USDA Natural Resources Conservation Service. Retrieved from https://websoilsurvey.sc.egov.usda.gov
Suyker, A. E. (2018a). AmeriFlux US-Ne1 Mead – Irrigated continuous maize site. http://dx.doi.org/10.17190/AMF/1246084
Suyker, A. E. (2018b). AmeriFlux US-Ne2 Mead – Irrigated maize-soybean rotation site. http://dx.doi.org/10.17190/AMF/1246085
Suyker, A. E. (2018c). AmeriFlux US-Ne3 Mead – Rainfed maize-soybean rotation site. http://dx.doi.org/10.17190/AMF/1246086
Stone, K. C., Bauer, P. J., & Sigua, G. C. (2016). Irrigation management using an expert system, soil water potentials, and vegetative indices for spatial applications. *Trans. ASABE, 59*(3), 941-948. https://doi.org/10.13031/trans.59.11550
Suyker, A. E., & Verma, S. B. (2009). Evapotranspiration of irrigated and rainfed maize-soybean cropping systems. *Agric. Forest Meteorol., 149*(3-4), 443-452. https://doi.org/10.1016/j.agrformet.2008.09.010
Suyker, A. E., Verma, S. B., Burba, G. G., Arkebauer, T. J., Walters, D. T., & Hubbard, K. G. (2004). Growing season carbon dioxide exchange in irrigated and rainfed maize. *Agric. Forest Meteorol., 124*(1-2), 1-13. https://doi.org/10.1016/j.agrformet.2004.01.011
Torres, E. A., & Calera, A. (2010). Bare soil evaporation under high evaporation demand: A proposed modification to the FAO-56 model. *Hydrol. Sci. J., 55*(3), 303-315. https://doi.org/10.1080/02626661003683249
Twine, T. E., Kustas, W. P., Norman, J. M., Cook, D. R., Houser, P. R., Meyers, T. P., ... Wesely, M. L. (2000). Correcting eddy-covariance flux underestimates over a grassland. *Agric. Forest Meteorol., 103*(3), 279-300. https://doi.org/10.1016/S0168-1923(00)00123-4
USDA. (2004). Chapter 10: Estimation of direct runoff from storm rainfall. In *National Engineering Handbook, Part 630 Hydrology*. Washington, DC: USDA Natural Resources Conservation Service. Retrieved from https://www.wcc.nrcs.usda.gov/ftpref/wntsc/H&H/NEHhydrology/ch10.pdf
USDA. (2012). USDA-FSA-APFO NAIP MrSID mosaic. Salt Lake City, UT: USDA Farm Service Agency, Aerial Photography Field Office. Retrieved from https://datagateway.nrcs.usda.gov
USDA. (2009a). Processed TIGER 2002 counties + NRCS additions dissolve. Fort Worth, TX: USDA-NRCS National Geospatial Center of Excellence. Retrieved from https://datagateway.nrcs.usda.gov
USDA. (2009b). Processed TIGER 2002 counties plus NRCS additions. Fort Worth, TX: USDA-NRCS National Geospatial Center of Excellence. Retrieved from https://datagateway.nrcs.usda.gov
USDOE. (2017a). AmeriFlux. Berkeley, CA: U.S. Department of Energy, Lawrence Berkeley National Laboratory. Retrieved from http://ameriflux.lbl.gov/
USDOE. (2017b). Site search: AmeriFlux network. Berkeley, CA: U.S. Department of Energy, Lawrence Berkeley National Laboratory. Retrieved from http://ameriflux.lbl.gov/sites/site-search/#filter-type=all
USDOE. (2017c). US-Ne1: Mead - irrigated continuous maize site. AmeriFlux. Berkeley, CA: U.S. Department of Energy, Lawrence Berkeley National Laboratory. Retrieved from http://ameriflux.lbl.gov/sites/siteinfo/US-Ne1
USDOE. (2017d). US-Ne2: Mead - irrigated maize-soybean rotation site. AmeriFlux. Berkeley, CA: U.S. Department of Energy, Lawrence Berkeley National Laboratory. Retrieved from http://ameriflux.lbl.gov/sites/siteinfo/US-Ne2
USDOE. (2017e). US-Ne3: Mead - rainfed maize-soybean rotation site. AmeriFlux. Berkeley, CA: U.S. Department of Energy, Lawrence Berkeley National Laboratory. Retrieved from http://ameriflux.lbl.gov/sites/siteinfo/US-Ne3
USGS. (2016). What are the band designations of Landsat satellites? Reston, VA: U.S. Geological Survey. Retrieved from https://landsat.usgs.gov/what-are-band-designations-landsat-satellites
Zreda, M., Shuttleworth, W. J., Zeng, X., Zweck, C., Desilets, D., Franz, T. E., & Rosolem, R. (2012). COSMOS: the cosmic-ray soil moisture observing system. *Hydrol. Earth Syst. Sci., 16*(11), 4079-4099. https://doi.org/10.5194/hess-16-4079-2012